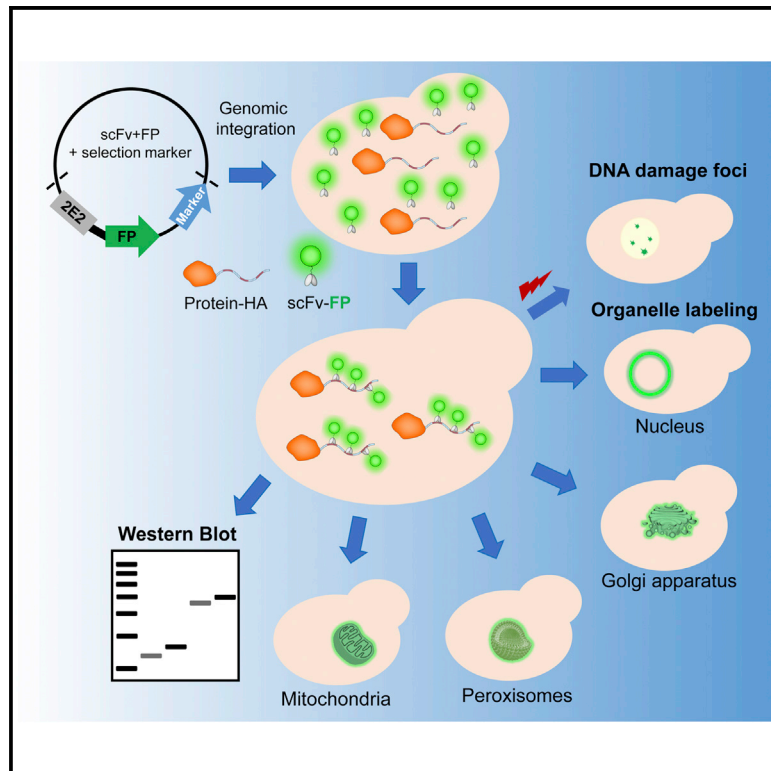


Protein fluorescent labeling in live yeast cells using scFv-based probes

Graphical abstract



Authors

Ioannis Tsirkas, Tomer Zur, Daniel Dovrat, Amit Cohen, Lior Ravkaie, Amir Aharoni

Correspondence

aaharoni@bgu.ac.il

In brief

Microscopy detection of cellular proteins is facilitated by their fusion to fluorescent proteins. However, cellular proteins that are expressed at low levels and/or are sensitive to fusions are hard to detect in live cells. To address this challenge, Tsirkas et al. develop an approach for the enhanced fluorescent labeling of HA-tagged yeast cellular proteins by scFv fused to fluorescent proteins.

Highlights

- Fluorescent labeling of HA-tagged proteins in yeast by scFv-fluorescent proteins
- Increased sensitivity of DNA-damage detection by HA-labeled Rfa1 and Rad52
- Efficient labeling of HA-tagged protein containing sensitive C'-terminal region
- Enhanced imaging of proteins localized to diverse cellular organelles



Article

Protein fluorescent labeling in live yeast cells using scFv-based probes

Ioannis Tsirkas,^{1,2} Tomer Zur,^{1,2} Daniel Dovrat,¹ Amit Cohen,¹ Lior Ravkaie,¹ and Amir Aharoni^{1,3,*}¹Department of Life Sciences and the National Institute for Biotechnology in the Negev, Ben-Gurion University of the Negev, Be'er Sheva 84105, Israel²These authors contributed equally³Lead contact*Correspondence: aaharoni@bgu.ac.il<https://doi.org/10.1016/j.crmeth.2022.100357>

MOTIVATION Microscopy studies of protein localization and function in living cells are facilitated by their fusion to fluorescent proteins. Low expression of cellular proteins and their C'-terminal sensitivity to fluorescent protein fusion render many of these proteins hard to detect in live cells. To overcome these limitations, we developed an approach for enhanced imaging of fluorescent proteins in live yeast cells by the binding of scFv-fluorescent protein fusion to multiple HA-tagged proteins. This approach enables highly sensitive DNA-damage detection, the facile labeling of C'-terminal sensitive proteins, and the enhanced detection of proteins localized to different cellular organelles.

SUMMARY

The fusion of fluorescent proteins (FPs) to endogenous proteins is a widespread approach for microscopic examination of protein function, expression, and localization in the cell. However, proteins that are sensitive to FP fusion or expressed at low levels are difficult to monitor using this approach. Here, we develop a single-chain fragment variable (scFv)-FP approach to efficiently label *Saccharomyces cerevisiae* proteins that are tagged with repeats of hemagglutinin (HA)-tag sequences. We demonstrate the successful labeling of DNA-binding proteins and proteins localized to different cellular organelles including the nuclear membrane, peroxisome, Golgi apparatus, and mitochondria. This approach can lead to a significant increase in fluorescence intensity of the labeled protein, allows C'-terminal labeling of difficult-to-tag proteins and increased detection sensitivity of DNA-damage foci. Overall, the development of a scFv-FP labeling approach in yeast provides a general and simple tool for the function and localization analysis of the yeast proteome.

INTRODUCTION

The budding yeast *Saccharomyces cerevisiae* is a bona fide model organism for studying eukaryotic biology,¹ and many conserved metabolic or signaling pathways were originally discovered in yeast.^{2,3} The research in *S. cerevisiae* was revolutionized by the discovery and utilization of fluorescent proteins (FP), allowing the function, expression, and localization analysis of specific proteins in live yeast cells as well as enabling the systematic studies of the entire yeast proteome.⁴⁻⁶ Furthermore, the development of enhanced and yeast-optimized (YO) versions of FPs, such as Envy and mKate2,^{7,8} has expanded the toolkit for protein studies in live yeast cells. Tagging of cellular proteins with repeats of various short tags, such as hemagglutinin (HA), FLAG, or MYC tags, followed by immunoassays⁹ is another common approach for assessing protein expression and localization in yeast. However, the usage of fluorescent microscopy and immunoassays for the examination of cellular proteins often

requires their independent fusion with FP and short tags, respectively, doubling the number of strains needed for comprehensive protein analysis.

While fluorescent labeling of proteins is an important tool for cell biology research, it is not applicable for all cellular proteins. Fusion of native proteins to FPs may lead to their mislocalization, aggregation, or impaired function, hindering their analysis in live cells.^{10,11} Moreover, the expression of some cellular proteins is extremely low, resulting in a low fluorescent signal, and thus requires the tandem fusion of more than one FP to facilitate their detection. To overcome these challenges, various tags labeled with bright small-molecule dyes were developed, including SNAPtag, CLIPtag, and HALOtag,¹²⁻¹⁴ and strategies for N'-terminal FP fusion were developed.¹⁵ However, dyes are prone to fast photobleaching upon continuous irradiation, and N' terminus labeling is challenging and can alter protein expression levels.¹⁵⁻¹⁷

Single-chain fragment variable (scFvs) domains of antibodies that bind specific epitopes in live cells have found multiple



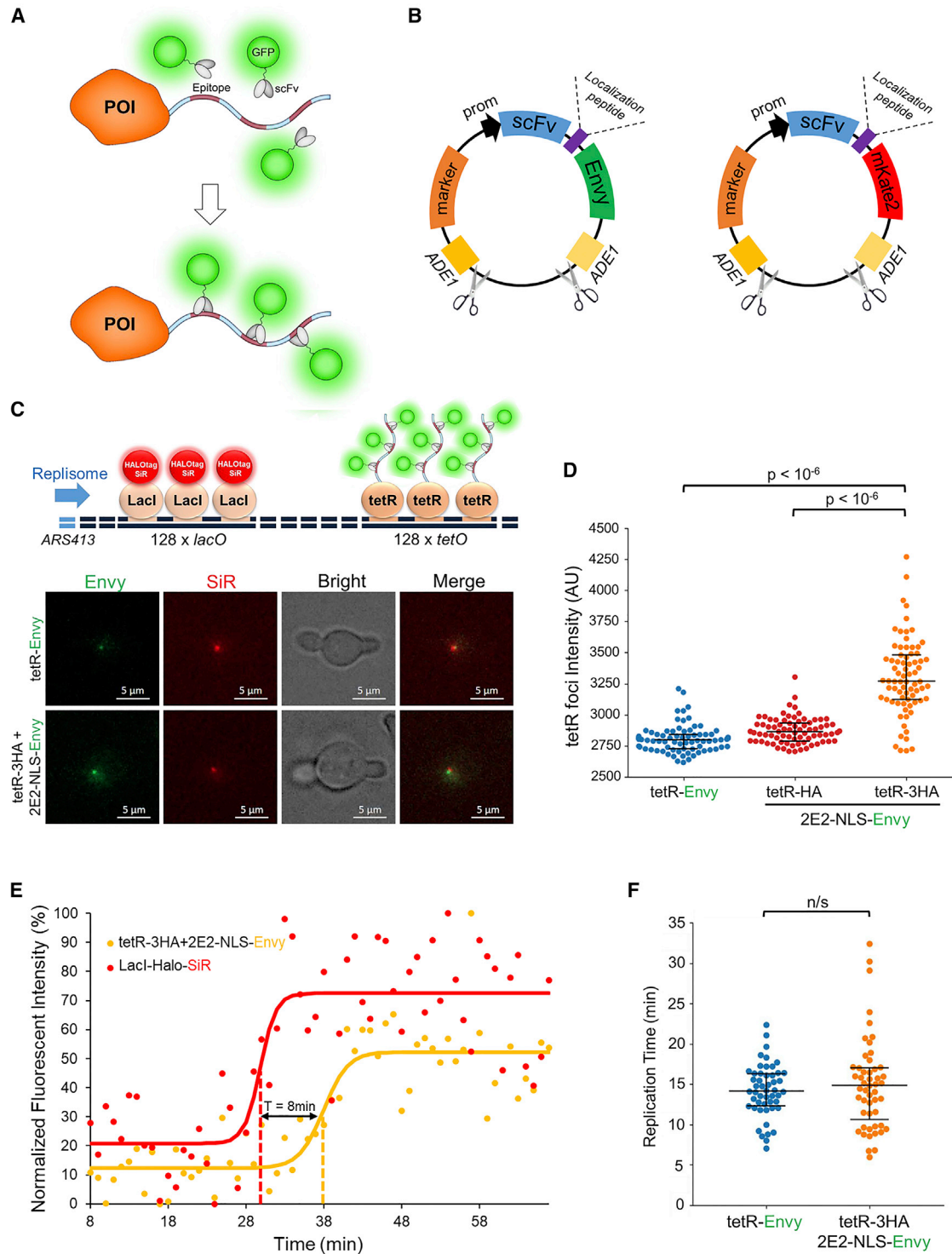


Figure 1. Design of the scFv system for the fluorescent labeling of tagged proteins and its application for imaging chromosomal loci in live yeast cells

(A) Schematic illustration of scFv-FP labeling of a tagged protein of interest (POI) in live yeast cells. Cells expressing scFv-FP (green) can label a POI (orange) tagged with short epitope sequences (red) in live cells.

(B) General plasmid design for the expression of scFv-Envy or scFv-mKate2 in live yeast cells. The scFv variants can be localized to different cellular compartments depending on the sequence of the localization peptide (purple). The scFv-FP variants are expressed under the control of either a weak *URA3* promoter

(legend continued on next page)

applications due to their small size and stability.¹⁸ Recently, the development of scFvs fused to FPs^{19–23} and the creation of arrays of epitope tags, namely “spaghetti monster FPs” (smFPs)²⁴ allowed the efficient labeling of a variety of cellular proteins. Nevertheless, while these approaches have found extensive usage in mammalian cells, scFvs were not utilized in yeast for the enhanced detection of epitope-labeled proteins.

In the current study, we developed a fluorescent scFv labeling approach of HA-tagged proteins in the yeast *S. cerevisiae* for the efficient labeling of diverse proteins while maintaining their function and cellular localization. We applied this approach for the fluorescent labeling of a fluorescent repressor-operator system (FROS), two DNA-damage markers, Rfa1 and Rad52, and proteins localized to different cellular organelles. In the case of DNA-damage markers, we show that the small size of the HA tag and low expression of the scFv enable maintenance of protein function and enhanced sensitivity compared with direct FP fusion. For HA-tagged proteins localized to different organelles including nuclear membrane, Golgi apparatus, and mitochondria, we show that increased expression of scFv leads to enhanced protein detection relative to direct GFP fusion. Overall, this system is highly versatile, allowing researchers to match scFv expression level to their target HA-fused protein for optimal cellular labeling. Our study can significantly contribute to researchers using yeast as a model organism, enabling the sensitive and efficient detection of proteins of interest for cell biology research.

RESULTS

System design and expression analysis of scFvs in *S. cerevisiae*

Our methodology is based on tagging a protein of interest (POI) with consecutive repeats of an epitope sequence and expressing the cognate scFv-FP, recognizing this specific epitope tag, in live yeast cells (Figure 1A). The possible binding of multiple copies of the fluorescent scFvs to the epitope-tagged protein can result in enhanced fluorescence detection while alleviating the need for tandem FP fusion (Figure 1A). To develop this approach in yeast, we initially chose three scFvs that were previously examined in mammalian cells: two scFvs binding to HA tag²² and the gp41 nanobody (gp41Nb) binding to a sequence derived from gp41, termed moon tag.¹⁹

To enhance the flexibility of the system, we fused the scFv to Envoy⁷ or yomKate2,⁸ which are YO versions of high-brightness

green and red FPs, respectively, and constructed variants of the scFv-FP for nuclear and cytoplasmic localization (Figure S1A). The expression of the scFv-FPs is controlled by a short version of the *URA3*, *RPL15A*, or *ADH1* promoter for obtaining low, medium, or high expression levels of the scFv-FP variants, respectively.²⁵ Finally, to allow easy integration of the scFv-FP fusion into yeast, we generated a series of selectable integrative plasmids targeting the scFvs into the *ADE1* locus (Figures 1B and S1A).

We initially fused the three scFvs, targeting HA tag (HA) or moon tag, to a nuclear localization signal (NLS)²⁶ and Envoy and expressed the scFv-NLS-Envoy in yeast under the control of the *URA3* promoter. We found that both HA-binding scFvs, 15F11-Envoy and 2E2-Envoy,²² are successfully expressed in the yeast nuclei; however, only 2E2-Envoy shows a homogeneous signal without forming non-specific fluorescent puncta (Figure S1B). In addition, gp41Nb-NLS-Envoy was successfully expressed, albeit with weaker nuclear intensity. In addition, we expressed 2E2-Envoy without the NLS, under the control of either the weak *URA3* or the stronger *RPL15A* promoter, and detected 2E2-Envoy throughout the cell body (Figure S1B). Importantly, none of the expressed scFvs significantly affected yeast cell growth (Figure S1C).

Enhanced functional labeling of chromosomal loci using scFv-FP

Next, we examined whether the scFvs-FP can be used for the specific labeling of epitope-tagged protein in the yeast nuclei. A common approach for labeling a specific DNA locus in the eukaryotic genome is by the FROS. The FROS is based on the integration of arrays of bacterial *lacO* and/or *tetO* sequences and the expression of their cognate fluorescently labeled LacI and/or tetR repressors, respectively.^{27–29} Using this system, the LacI/tetR-labeled chromosomal locus is visible under fluorescent microscopy as distinct fluorescent dots.²⁷ To examine the ability of the scFv approach to label a *tetOx128* array in the yeast genome, we tagged tetR with HA- or moon-tag epitopes in strains expressing the cognate scFv-Envoy (Figures 1C and S1D). We found that in these cells, strong fluorescent nuclear foci were observed that colocalize with adjacent *lacOx128* array foci, labeled with LacI-Halo-SiR (Figure 1C). Comparison of *tetOx128* foci intensities in the different tetR-HA strains revealed that foci in the tetR-3HA cells were significantly brighter than those detected in cells expressing tetR fused to a single HA tag (tetR-HA) or tetR directly fused

to ensure low expression levels or stronger *RPL15A* or *ADH1* promoters for higher expression. The plasmids are digested with a restriction enzyme and integrated into the *ADE1* locus, and transformants are selected with an antibiotic selection marker. See Figure S1A for plasmid scheme.

(C) Top: schematic illustration of tetR-3HA bound by 2E2-NLS-Envoy for the labeling of a *tetOx128* array, which is located adjacent to a *lacO* array, labeled with LacI-Halo-SiR. Bottom: fluorescent foci of tetR-Envoy or tetR-3HA labeled with 2E2-NLS-Envoy bound to the *tetOx128* array (green) and LacI-Halo-SiR bound to the *lacOx128* array (red) rendering the chromosomal loci visible under the microscope as two colocalizing fluorescent foci. Z-plane orthogonal projections of 3D cell images are shown.

(D) Comparison of median tetR foci intensity in cells expressing tetR-Envoy or tetR-HA or tetR-3HA labeled with 2E2-NLS-Envoy expressed from the weak *URA3* promoter. For each strain, 76 cells were quantified.

(E) Representative single-cell analysis showing the increase in fluorescent intensity of the LacI-Halo-SiR (red) and labeled tetR-3HA (orange) foci due to *lacO* and *tetO* array duplication during DNA replication from *ARS413*. Solid lines represent a fit of the data to a sigmoidal function, and SiR-HALO and Envoy midpoints are indicated with dashed lines.

(F) Replication times of strains containing tetR-Envoy (blue, 50 cells) or labeled tetR-3HA (orange, 51 cells) showing no significant difference in replication times. Replication times measure the time delay between duplication of the *lacO* array and the *tetO* array, indicating fork progression rate.

to Envy (tetR-Envy) (Figure 1D). These results suggest that multiple copies of 2E2-NLS-Envy can label the tetR-3HA bound to the *tetOx128* array.

In contrast, we found that labeled tetR-3xMoontag foci were not brighter relative to the tetR-Envy foci (Figure S1E). In order to test whether increased expression of gp41Nb-NLS-Envy could enhance the fluorescent intensity of the tetR-3xMoontag foci, we generated a yeast codon-optimized version of gp41Nb-NLS-Envy and expressed the new construct in yeast cells containing *tetOx128*. Although the overall fluorescent signal of the YO gp41Nb was increased compared with the respective non-optimized version, this did not result in an increase of tetR-3xMoon-tag foci intensity (Figure S1D). Thus, we did not further develop the gp41Nb-FP as a general tool for FP labeling in yeast.

To examine the functionality of the labeled tetR-3HA, we utilized the *tetOx128*- and *lacOx128*-containing strain for monitoring replication fork progression, as previously described.²⁷ The replication of the *lacO* and *tetO* array by the replisome arriving from the *ARS413* leads to the recruitment of additional labeled repressors, resulting in the increase of fluorescent dot intensity. By monitoring fluorescent dot intensities in real time and measuring the time difference between the fluorescence increase midpoints of the two foci, a replication rate of single replisomes through the arrays can be calculated (Figure 1E).^{27,30–32} Using this approach, we found that tetR-3HA labeled with 2E2-NLS-Envy allows monitoring *tetO* array duplication (Figure 1E). Measuring fork progression in these cells revealed similar replication times as the respective tetR-Envy strain (Figure 1F), demonstrating that 2E2-NLS-Envy tetR-3HA labeling can be used for the enhanced imaging of chromosomal loci in live yeast cells, as well as for monitoring replisome progression.

C'-terminal 2E2-Envy labeling of Rfa1-HA variants maintains Rfa1 function and enhances DNA-damage detection

To expand the application of 2E2-Envy labeling in yeast, we applied this system for the fluorescence detection of DNA damage. One of the most common proteins used for the detection of DNA damage in eukaryotes is Rfa1.^{33,34} Rfa1 is a member of the heterotrimeric RPA protein complex that binds single-stranded DNA (ssDNA) at sites of DNA damage.^{35,36} While Rfa1 was previously fused to GFP at the C' terminus (Rfa1-GFP),^{37,38} it was demonstrated that such GFP fusion impairs Rfa1 function and compromises cell viability under DNA-damaging conditions.^{39,40} This probably stems from the importance of the Rfa1 C' terminus for DNA binding and RPA complex trimerization.⁴¹ We hypothesized that fusion of Rfa1 C' terminus to short HA tags would allow efficient Rfa1 fluorescent labeling by 2E2-Envy while maintaining its functionality as a sensitive sensor of DNA damage. Thus, we first examined whether tagged Rfa1-3HA or Rfa1-6HA leads to growth defects on agar plates containing a methyl methanesulfonate (MMS) alkylating agent relative to non-tagged strains.⁴² We found that while Rfa1-3HA and Rfa1-6HA tagged strains showed no growth defect, the Rfa1-Envy strain grew significantly slower in the presence of MMS (Figures 2A and S2A), in agreement with previous studies.^{39,40} These results highlight that the small and flexible HA tagging of the Rfa1 C' terminus al-

lows maintaining protein function under DNA-damaging conditions.

Next, we examined the ability of Rfa1-HA and 2E2-Envy to form RPA foci upon induction of DNA damage with short-wavelength irradiation. We chose to examine strains expressing 2E2-Envy under the weak *URA3* promoter for reducing the 2E2-Envy nuclear background. We found that while all strains exhibit a low basal level of RPA foci in the absence of DNA damage, upon induction of DNA damage, a significant increase in RPA-foci-containing cells was detected (Figures 2B, 2C, and S2B). Interestingly, we observed an increase of more than 2-fold in the percentage of cells containing RPA foci in the labeled Rfa1-3HA or Rfa1-6HA cells compared with direct Rfa1-Envy fusion (Figure 2C). While Rfa1-Envy foci were also detected in the cytoplasm (Figure S2C) as previously reported,⁴³ foci of Rfa1-3HA and Rfa1-6HA labeled with 2E2-NLS-Envy were localized exclusively to the nucleus (Figure S2D). Quantitative analysis of Envy fluorescent intensities revealed that both RPA foci intensities and nuclear fluorescent background are weaker in cells expressing Rfa1-3HA or Rfa1-6HA labeled with 2E2-NLS-Envy relative to Rfa1-Envy cells (Figures S2E and S2F). These results suggest that the enhanced detection of RPA foci in the Rfa1-HA strains stems from low 2E2-NLS-Envy nuclear background, enabling improved detection of weak foci. We did not observe enhanced foci intensity in Rfa1-6HA relative to Rfa1-3HA, suggesting that the low level of 2E2-Envy and/or the high sensitivity of the Rfa1 C' terminus restrict the number of bound 2E2-Envy proteins. Attempts to increase RPA foci intensity by expressing 2E2-NLS-Envy from the stronger *RPL15A* promoter led to increased non-specific fluorescent foci observed prior to DNA-damage induction (Figures S2G). Next, we examined the labeling of Rfa1-3HA and Rfa1-6HA in strains expressing 2E2-Envy without NLS peptide. We found that following DNA damage induction in Rfa1-3HA strain, RPA foci levels were similar to the Rfa1-Envy strain (Figure 2C) and upon high illumination cytosolic Rfa1 foci could be detected (Figure S2C). Finally, we used WB analysis to detect Rfa1-3HA and Rfa1-6HA expression in these strains (Figure 2D), demonstrating the dual usage of the Rfa1-HA strains for fluorescence imaging and WB analysis.

Overall, these results show the applicability of 2E2-NLS-Envy for the C' terminal labeling of HA-tagged Rfa1 while maintaining its function. Our results demonstrate that while the Rfa1-HA labeling with 2E2-NLS-Envy doesn't enhance the intensity of RPA foci (Figure S2F), it significantly enhances the sensitivity of DNA damage detection, relative to Rfa1-GFP fusion (Figure 2C). These results highlight the importance of low 2E2-NLS-Envy expression level, which is independent of Rfa1 expression, for achieving improved sensitivity of DNA damage detection in live cells.

Enhanced DNA double-strand break (DSB) detection using fluorescently labeled Rad52-HA

A frequently used protein for the detection of double strand breaks (DSBs) in live eukaryotic cells is Rad52.^{44–46} Rad52 generates a multimeric protein complex at DSB sites catalyzing the homologous pairing reaction of the two DSB ends.⁴⁷ To examine whether 2E2-Envy can be utilized for the sensitive detection of

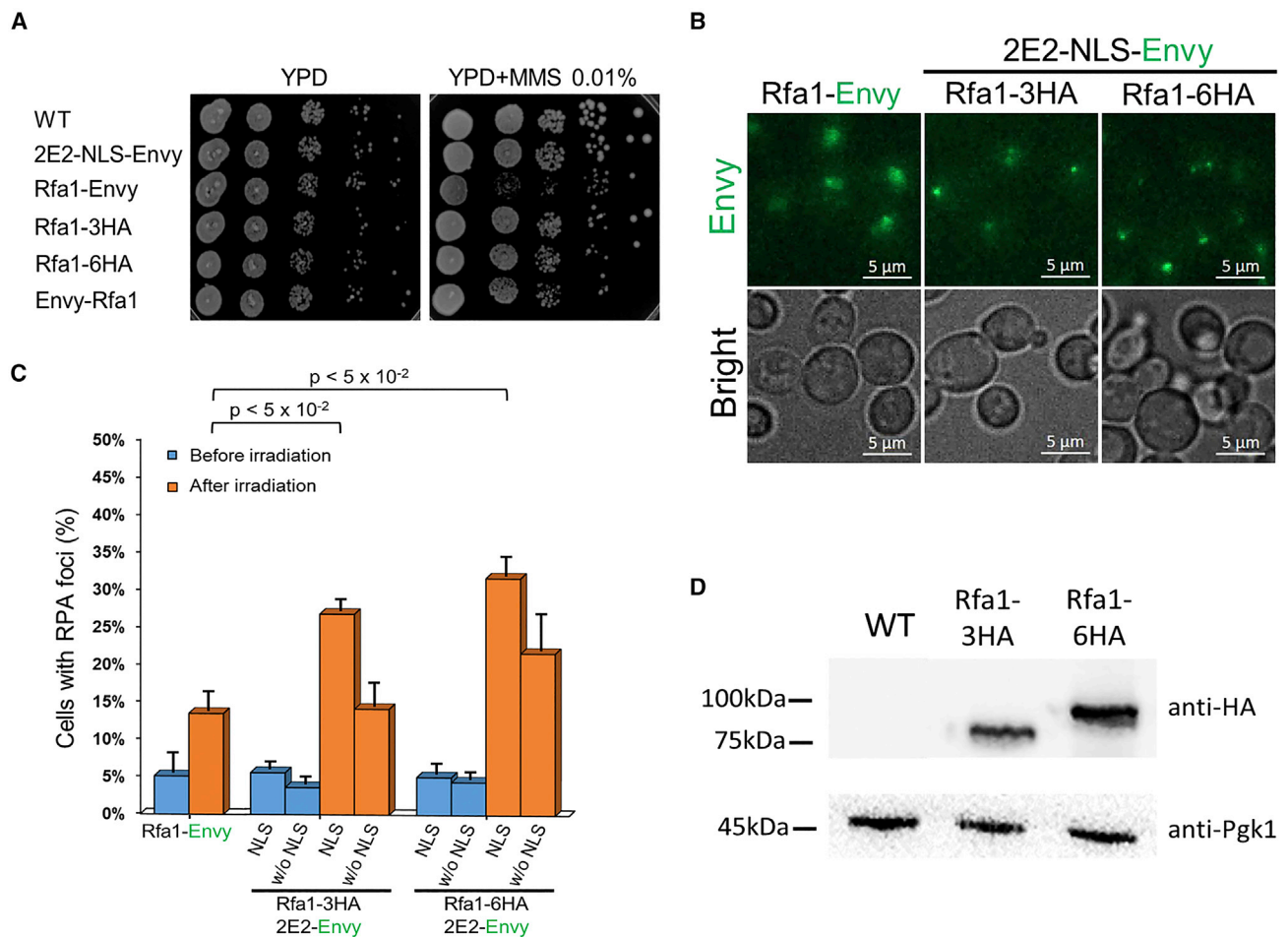


Figure 2. Labeling of Rfa1-HA by 2E2-NLS-Envy maintains Rfa1 functionality and leads to enhanced detection of RPA foci

(A) Phenotypic analysis of yeast strains expressing different versions of tagged Rfa1 including strains expressing Rfa1-3HA or Rfa1-6HA and 2E2-NLS-Envy expressed from the weak *URA3* promoter. Spot growth assay on YPD agar plates with or without MMS indicates a phenotypic defect in a strain expressing C'-terminal Rfa1-Envy grown in the presence of MMS.

(B) Representative images of RPA foci in cells expressing Rfa1-Envy or Rfa1-HA labeled with 2E2-NLS-Envy, following DNA-damage induction. Lower nuclear fluorescent background is observed in labeled Rfa1-HA cells relative to Rfa1-Envy cells (see Figure S2E for quantification). Z-plane orthogonal projections of 3D cell images are shown.

(C) Enhanced detection of RPA foci upon DNA-damage induction in strains expressing Rfa1-HA labeled with 2E2-NLS-Envy relative to the Rfa1-Envy strain. Rfa1-HA labeling with 2E2-Envy without NLS did not lead to enhanced detection of RPA foci relative to Rfa1-Envy. Results represent an average of three independent repeats, and error bars represent the standard error of the mean (SEM). At least 240 cells were examined in each experiment.

(D) Detection of Rfa1 expression in the labeled Rfa1-HA strains using WB analysis showing the dual usage of these strains for microscopy and WB analysis. PGK1 examination is used as an internal control. In all Rfa1-HA-labeled strains, 2E2-Envy is expressed from the weak *URA3* promoter.

DSB sites in live cells, we examined Rad52 foci in strains expressing Rad52-3HA or -6HA variants and 2E2-Envy, relative to Rad52-Envy strain. In these strains, we measured the number of Rad52 foci (Figure 3A) before and after induction of DNA damage (Figure 3B), as performed for the Rfa1 experiments. While the number of foci detected prior to irradiation was similar in all strains, upon induction of DNA damage we detected a significant increase in Rad52 foci appearance in the labeled Rad52-3HA and Rad52-6HA strains, compared to Rad52-Envy strain (Figures 3B, S3A and S3B). We found that this increase in Rad52 foci formation was more profound in cells expressing Rad52-HA variants labeled with 2E2-Envy without an NLS

sequence (Figure 3B). Notably, the increase in Rad52 foci detected in these strains is correlated with reduced nuclear fluorescent background, allowing the identification of weak Rad52 foci (Figures S3C and S3D). Next, we validated the functionality of Rad52-HA strains (Figure S3E) and performed western blot (WB) analysis for the analysis of Rad52 expression levels, showing the dual usage of these strains for fluorescent imaging and WB analysis (Figure S3F).

Finally, to verify that the fluorescent foci detected in the labeled Rad52 strains are genuine Rad52 foci, we introduced a second copy of Rad52 fused to mKate2 (Figure 3C). Indeed, we found that foci of Rad52-3HA and Rad52-6HA labeled with

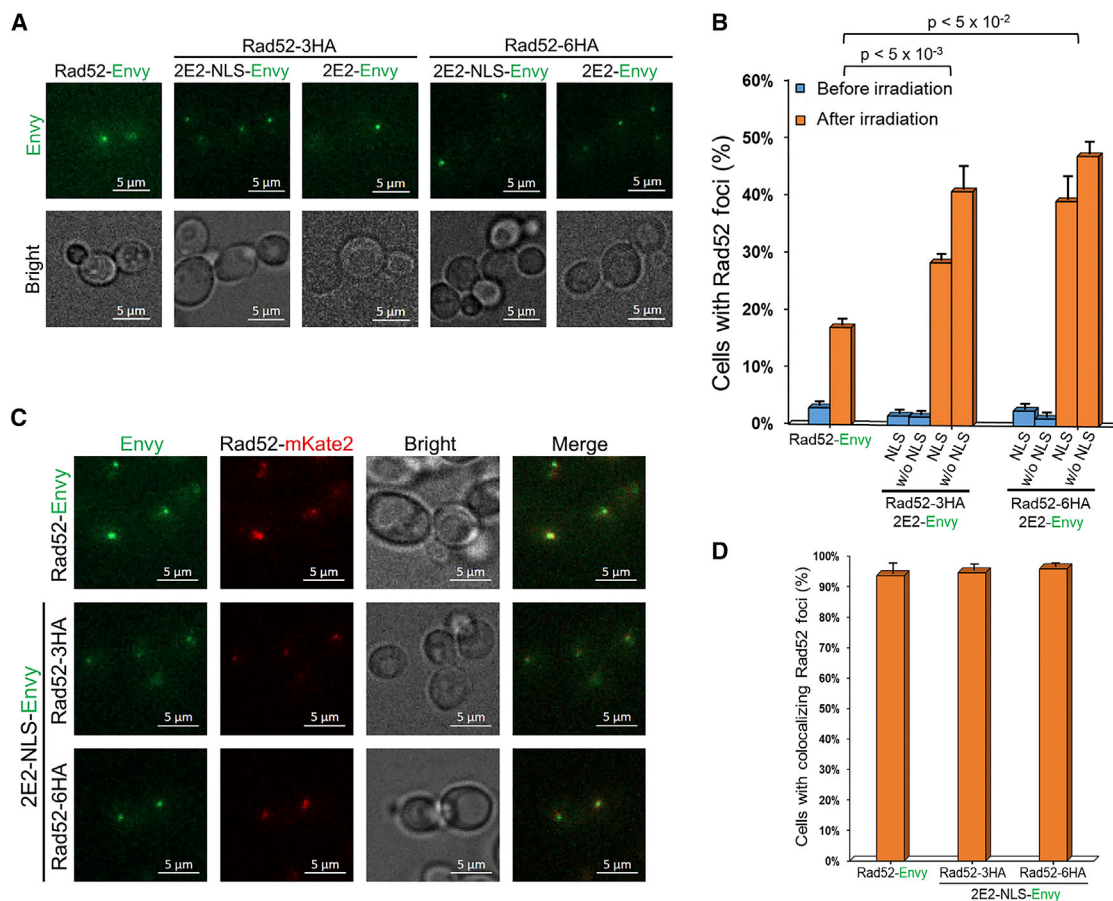


Figure 3. Enhanced detection of DSBs in strains expressing Rad52-HA labeled with 2E2-Envy

(A) Representative Rad52 foci following DNA-damage induction in strains expressing Rad52-Envy or Rad52-HA variants labeled with 2E2-Envy expressed from the weak *URA3* promoter.

(B) Higher sensitivity of Rad52 foci detection following DNA-damage induction in the labeled Rad52-HA strains relative to the Rad52-Envy strains.

(C) Representative Rad52 foci in strains expressing labeled Rad52-HA variants and a second copy of Rad52-mKate2. Envy foci colocalize with Rad52-mKate2 foci, validating Rad52 foci detection.

(D) Percentage of cells containing colocalized labeled Rad52-HA and Rad52-mKate2 foci.

Results for (B) and (D) are the average of three independent repeats, and error bars are SEM. At least 150 cells were examined in each experiment. In all Rad52-HA-labeled strains, 2E2-Envy is expressed under the weak *URA3* promoter. In (A) and (C), Z-plane orthogonal projections of 3D cell images are shown.

2E2-NLS-Envy colocalize with the Rad52-mKate2 foci in more than 95% of the cells (Figure 3D). Overall, these results show that 2E2-Envy labeling can significantly enhance the detection of Rad52-HA foci for the sensitive examination of double-stranded breaks (DSBs) in live yeast cells.

Fluorescent labeling of HA-tagged nuclear pore complex (NPC)

To investigate whether 2E2-Envy can be used for the labeling of HA-tagged non-DNA-binding proteins, we utilized strains expressing cytoplasmic 2E2-Envy under the control of the weak *URA3* promoter or the stronger *RPL15A* promoter. First, we examined whether we could use the cytoplasmic 2E2-Envy to label HA-tagged proteins located in the NPC in order to detect the periphery of the yeast nucleus. NPCs mediate the transport and exchange of small molecules and proteins between the nucleus and the cytoplasm of the cell.⁴⁸ These complexes are

composed of many different proteins called nucleoporins (Nups) spanning the whole nuclear membrane.⁴⁹ To examine whether HA-tagged NPCs can be visualized in live yeast cells using cytoplasmic 2E2-Envy, we labeled two different Nups, Nup157 and Nup159, located in the nuclear interior region and in the cytoplasmic interface, respectively.⁴⁹ We found that in cells expressing HA-tagged Nup157 and Nup159 and 2E2-Envy, the nuclear periphery was clearly visualized as clear fluorescent rings, similar to the direct Nup157-Envy and Nup159-Envy cells (Figures 4A and 4B). Importantly, we discovered that higher expression of 2E2-Envy leads to a significant increase in the fluorescence intensity of HA-tagged Nup157 and Nup159 relative to the respective direct Envy fusion proteins or the respective labeling with 2E2-Envy expressed from the weak *URA3* promoter (Figures 4A and 4B). Quantitative analysis of the Nup fluorescence intensity indicates an around 3-fold increase in the intensity of Nups-HA variants

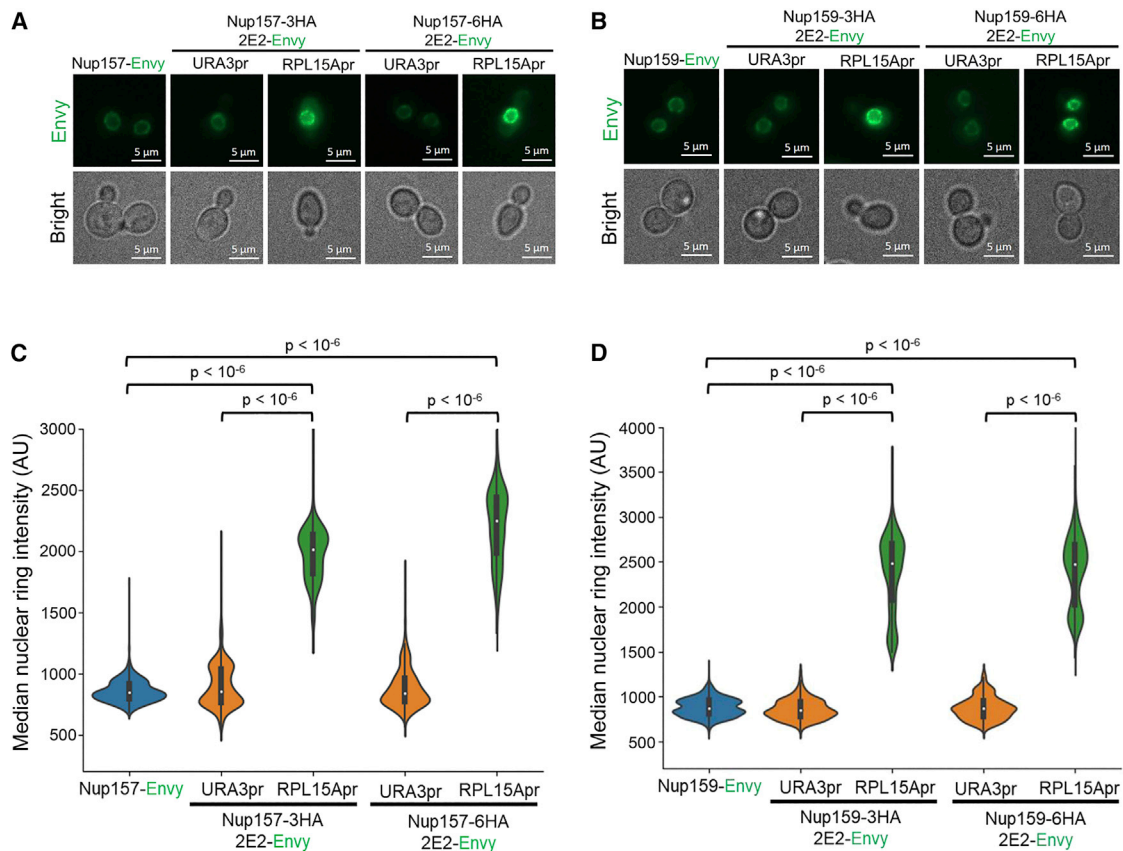


Figure 4. Enhanced imaging of nucleoporins in live yeast cells using Nup-HA variants labeled with 2E2-Envy

(A and B) Representative images of cells expressing Nup157-Envy or Nup157-HA variants (A) and Nup159-Envy or Nup159-HA variants (B) labeled with 2E2-Envy expressed from the weak *URA3* promoter or the stronger *RPL15A* promoter. Single Z-plane cell images are shown.

(C and D) Quantification of fluorescent nuclear ring intensities of Nup157-Envy or labeled Nup157-HA variants (C) and Nup159-Envy or labeled Nup159-HA variants (D) in strains expressing 2E2-Envy under the control of either *URA3* or *RPL15A* promoter. Number of cells analyzed for Nup157-Envy is 1,083, Nup157-3HA are 1,529 and 1,172, and Nup157-6HA are 1,139 and 955 for 2E2-Envy expressed under *URA3pr*- and *RPL15Apr*, respectively. Number of cells analyzed for Nup159-Envy is 904, Nup159-3HA are 1,062 and 1,035, and Nup159-6HA are 838 and 1,097 for 2E2-Envy expressed from *URA3pr*- and *RPL15Apr*, respectively.

labeled with 2E2-Envy expressed under the stronger *RPL15A* promoter relative to the direct Nup-Envy fusions (Figures 4C and 4D). These results indicate that about three 2E2-Envy proteins bind and label the Nup-HA variants, allowing enhanced detection of the protein in the nuclear periphery.

To expand the possibility of labeling cellular proteins with different FPs, we constructed plasmids expressing 2E2-mKate2 for the labeling of HA-tagged proteins with red FPs (Figure S1A). Using 2E2-mKate2, we efficiently labeled the Nup157-HA and Nup159-HA variants, visualized as clear fluorescent rings (Figure S4), allowing the red fluorescent visualization of the nuclear periphery. Finally, we examined the growth of the labeled Nup-HA strains and found a slower growth rate of Nup-6HA strains relative to the Nup-3HA strain or Nup-Envy fusion (Figures S4E and S4F), indicating that it is preferable to use the Nup-3HA for fluorescent labeling by the 2E2-Envy. Overall, these results demonstrate that HA-tagged proteins can be efficiently labeled with different 2E2-FP for enhanced and versatile protein detection in live cells.

Fluorescent labeling of HA-tagged peroxisomes, Golgi, and mitochondrial proteins

Next, we tested whether we could exploit 2E2-FP approach for the labeling of proteins located in other cellular organelles. We initially labeled the yeast peroxisome, which is composed of multiple peroxin (Pex) proteins that are involved in diverse metabolic functions.⁵⁰ We chose to label Pex3 protein, which is a member of the importomer complex located on the peroxisomal membrane, responsible for protein translocation inside the peroxisome core.⁵¹ We labeled Pex3-HA variants with 2E2-Envy or 2E2-mKate2 expressed from the weak *URA3* promoter and observed green or red foci, respectively, similar to Pex3-Envy foci (Figures 5A and S5A). Quantification of the 2E2-Envy-labeled Pex3-HA foci revealed a significant increase in intensity relative to foci formed by direct Pex3-Envy fusion (Figure S5B) and a mild decrease in foci intensity of 2E2-mKate2-labeled Pex3-6HA relative to Pex-3HA (Figure S5C). To validate that the foci seen in Pex3-HA strains are indeed labeled peroxisomes, we fused a second peroxisomal protein,

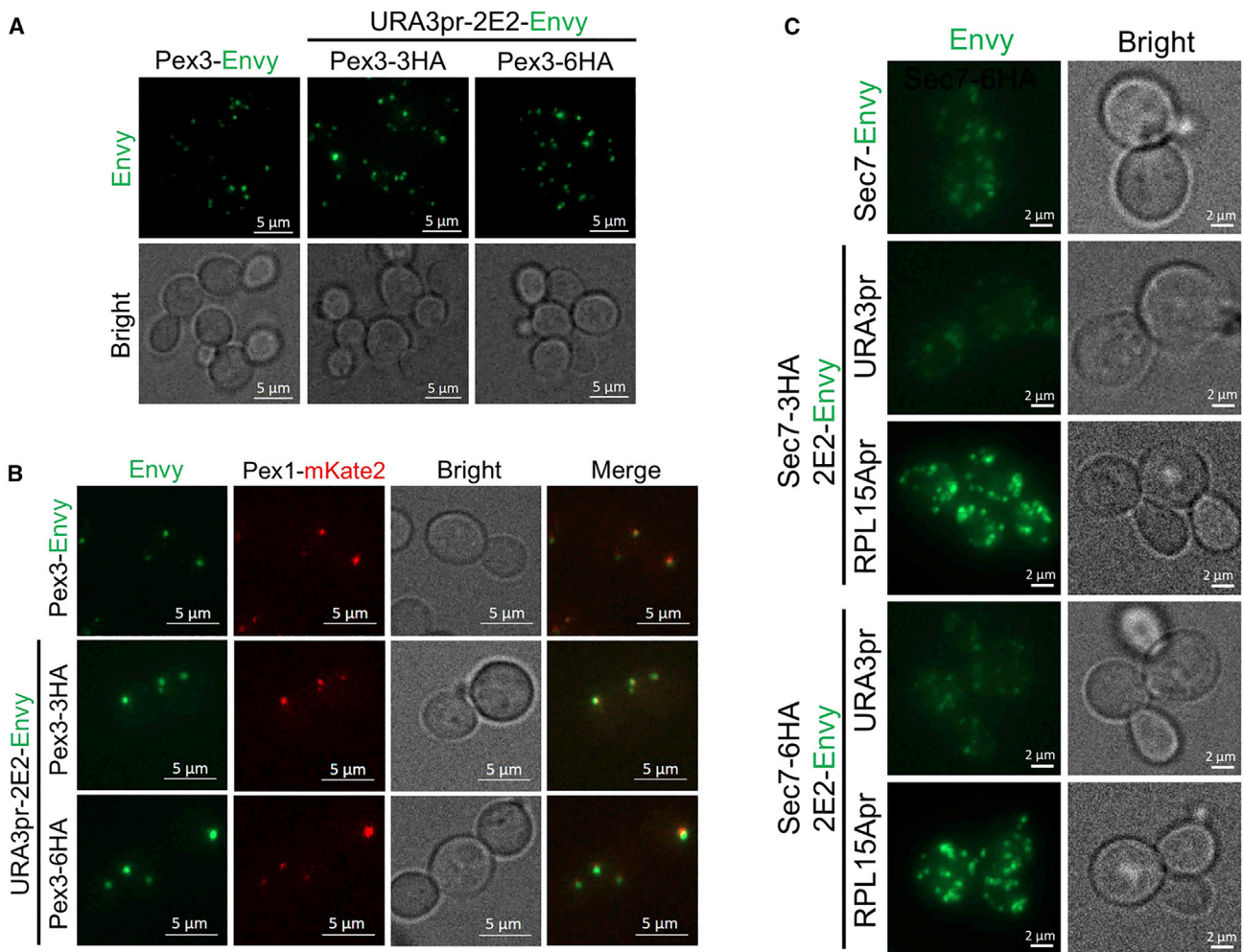


Figure 5. Imaging of peroxisomes and Golgi apparatus in live yeast using Pex3-HA and Sec7-HA variants, respectively, labeled with 2E2-Envy
(A) Representative images of cells expressing Pex3-Envy or Pex3-HA variants labeled with 2E2-Envy expressed from the weak *URA3* promoter showing multiple peroxisomal foci.
(B) Colocalization of labeled Pex3-HA foci with Pex1-mKate2 foci validating the correct localization of the labeled Pex3-HA foci to peroxisomes.
(C) Representative images of cells expressing Sec7-Envy or Sec7-HA variants labeled with 2E2-Envy expressed from the weak *URA3* promoter or the stronger *RPL15*pr, showing multiple Golgi puncta. A significant increase of puncta intensity is observed for strains expressing 2E2-Envy from *RPL15*Apr relative to Sec7-Envy or Sec7-HA labeled with 2E2-Envy expressed from the weak *URA3* promoter. Quantification of peroxisome and Golgi foci intensities are shown in Figures S5B and S5G, respectively. Z-plane orthogonal projections of 3D cell images are shown.

Pex1, to mKate2 on the background of Pex3-HA and Pex3-Envy strains.⁵² We found that foci of Pex3-HA variants labeled with 2E2-Envy colocalize with Pex1-mKate2 foci (Figure 5B), demonstrating that the scFv labeling of Pex3-HA maintains correct protein localization. To verify that HA labeling of Pex3 does not reduce protein function, we examined the growth of these strains on plates containing oleic acid as a carbon source.⁵³ We found that Pex3-HA and 2E2-Envy strains did not show any growth defects, relative to the sensitive *Pex6Δ* strain,⁵² highlighting the potential of the system for labeling peroxisomal proteins (Figure S5D). In our attempts to further increase the intensity of HA-tagged Pex3 foci, we generated and examined strains expressing 2E2-Envy from the stronger *RPL15A* promoter. However, in the case of Pex3-HA strains, the increased

expression of 2E2-Envy led to large non-specific puncta (Figure S5E).

To visualize the Golgi apparatus, we used the 2E2-Envy to label Sec7-HA variants.⁵² Sec7 is a large, characteristic Golgi protein that is commonly used for imaging of the Golgi organelle.⁵² We found that upon labeling of Sec7-HA variants with 2E2-Envy, expressed from the stronger *RPL15A* promoter, no yeast growth defects were observed (Figure S5F), and clear strong puncta were visible, similar to puncta formed by Sec7-Envy (Figure 5C). We found that puncta intensity of the labeled Sec7-HA variants was significantly higher than the puncta detected in the Sec7-Envy cells (Figure S5G). In addition, we found that labeling of Sec7-HA variants with 2E2-Envy expressed from the weak *URA3* promoter

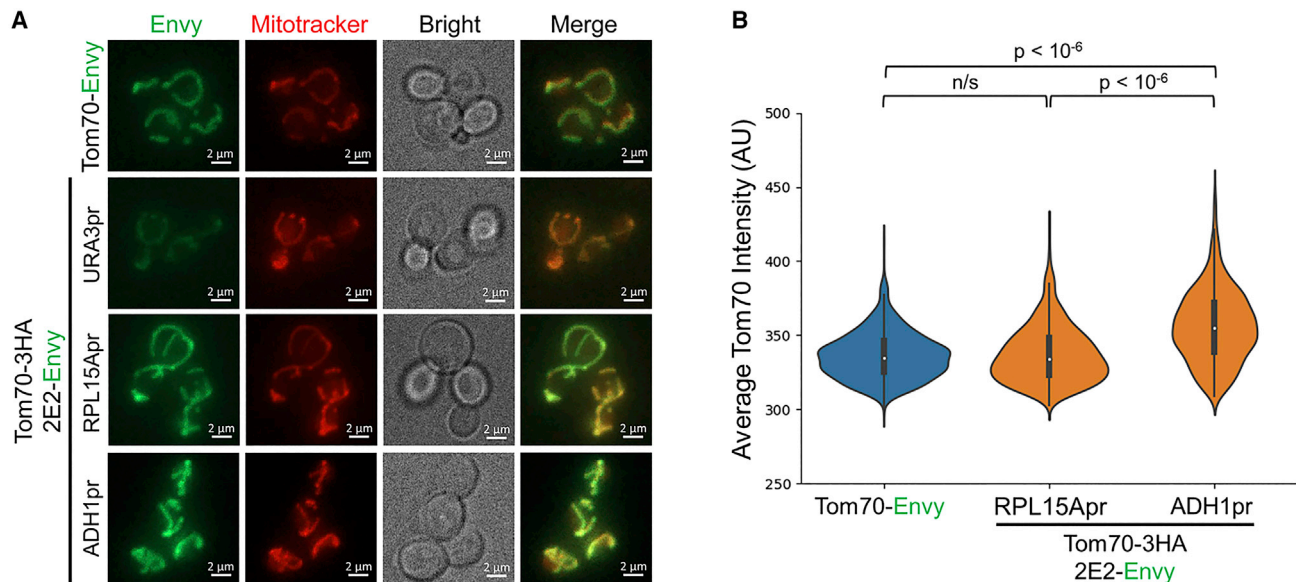


Figure 6. Imaging of mitochondria in live yeast cells using Tom70-HA variants labeled with 2E2-Envy

(A) Representative images of cells expressing Tom70-3HA labeled with 2E2-Envy expressed from different promoters and cells expressing Tom70-Envy. Colocalization of Mitotracker red CMXRos with the Envy signal verifies the correct labeling of mitochondria in the Tom70-3HA strains. Z-plane orthogonal projections of 3D cell images are shown.

(B) Tom70-3HA labeling with 2E2-Envy expressed from the *ADH1pr* results in stronger mitochondrial fluorescent intensity relative to direct Tom70-Envy or Tom70-3HA labeling with 2E2-Envy expressed from the *RPL15Apr*. Tom70-3HA labeling with 2E2-Envy expressed from the weak *URA3* promoter leads to a low signal that is below the detection threshold of our signal quantification approach. Number of cells analyzed is 696 for Tom70-Envy and 335 or 435 for Tom70-3HA labeled with 2E2-Envy expressed from *RPL15Apr* or *ADH1pr*, respectively.

showed significantly lower puncta fluorescent intensity (Figure S5G).

Finally, we used the 2E2-Envy system for the labeling of mitochondrial proteins focusing on HA-tagged Tom70. Tom70 is part of the translocase of outer membrane (TOM) complex that is involved in the recognition and initial import of proteins that are directed to the mitochondria.^{54,55} The TOM complex acts as a receptor for precursor proteins reaching the mitochondria.^{54,55} While labeling of Tom70-HA with 2E2-Envy expressed from the weak *URA3* promoter led to very low signal, labeling of Tom70-HA with 2E2-Envy expressed from the stronger *RPL15A* promoter led to very clear and characteristic mitochondrial labeling (Figures 6A and S6A). To verify that labeling of Tom70-HA with the 2E2-Envy indeed labels the mitochondria, we used the MitoTracker red CMXRos dye.⁵⁶ This red-fluorescent dye specifically stains the mitochondria in live cells and was extensively used in yeast and mammalian cells.^{56,57} In accordance with Tom70-HA localization to the mitochondria, we observed a clear colocalization of labeled Tom70-HA with the MitoTracker dye (Figures 6A and S6A). Analysis of the labeled Tom70-6HA fluorescent intensity revealed a small increase relative to the intensity of the Tom70-Envy-labeled protein (Figure S6B). To further increase the efficiency of Tom70-HA labeling by 2E2-Envy, we expressed 2E2-Envy from a very strong *ADH1* promoter (Figure 6A). We found that further increase in 2E2-Envy expression level led to increased fluorescent intensity of Tom70-3HA signal relative to the Tom70-Envy signal (Figure 6B). Finally, to verify that Tom70-HA-labeled cells sustain functional mitochondria, we assayed the growth of the strains on

plates containing glycerol as a carbon source.⁵⁸ We found that all strains exhibit normal growth relative to the *mdm38Δ* cells serving as a negative control⁵⁹ (Figure S6C).

Overall, these results highlight the importance of matching the 2E2-Envy expression level to the target HA-tagged protein for optimal fluorescent labeling. The efficient labeling of nuclear membrane proteins, peroxisome, Golgi, and mitochondria organelles using the HA-tagging and 2E2-FP approach demonstrates the wide potential of this system for the enhanced detection of different cellular proteins in yeast while maintaining their function and cellular localization.

DISCUSSION

Here, we developed scFv probes for the fluorescent imaging of tagged cellular proteins in live yeast cells. Using this approach, cellular proteins that are fused to commonly used tags, such as the HA tag, can be readily labeled by the cognate scFv-FP, allowing sensitive monitoring of protein function and localization inside the yeast cell. Fusion of a target protein to tandem tags enables its labeling with multiple scFv-FP proteins, thus leading to enhanced fluorescence intensity relative to direct protein-FP fusion. We have demonstrated the application of this approach for the labeling of different POI-HA located in different organelles in the cell. Specifically, we showed a significant increase in foci intensity of labeled *tetO* array, nuclear pore proteins, Golgi, and mitochondrial proteins relative to the respective direct protein-Envy fusions (Figures 1, 4, 5, and 6). An alternative strategy for enhanced fluorescent labeling of proteins in cells could be

achieved by fusion of three copies of GFP. However, this approach is technically challenging and can lead to loss of GFP repeats due to recombination.

We found that the expression level of scFv-FP plays a critical role for enhanced protein-HA labeling in the cell. Thus, for optimal labeling of 3HA-tagged protein, the expression level of the target protein and the scFv-FP should be considered (Table S1). In the analysis of different POI-HA variants, we observed no significant increase in the fluorescent intensity of labeled POI-6HA relative to POI-3HA proteins regardless of 2E2-Envy expression levels. It is possible that POI-6HA proteins are unable to bind more than three 2E2-Envy molecules due to negative cooperativity. In this case, binding of up to three 2E2-Envy molecules to the POI-6HA leads to dramatically reduced binding affinity of additional 2E2-Envy molecules to the tagged proteins. Thus, for practical applications, the usage of 3xHA tag is superior for fluorescent labeling of the target proteins we examined.

In our study, we demonstrated the application of scFv-FP in yeast for labeling of tagged Rfa1 and Rad52 for the sensitive detection of DNA damage and for labeling proteins localized to different cellular organelles. Previous studies in mammalian cells developed and applied scFvs and Fabs for monitoring protein posttranslational modifications (PTMs) and translation in live cells.^{21,60–64} Utilizing Fabs, the detailed kinetics of histone and RNA polymerase II PTMs were described during active transcription.⁶⁵ In addition, several studies have utilized scFvs for the detailed monitoring of protein translation while simultaneously labeling the translated RNA transcript in live cells.^{21,61–64} Our development of the scFv approach in yeast, combined with the facile labeling of individual mRNAs,^{32,66} highlight the potential for further development of the scFv approach for monitoring protein translation in live yeast cells.

Our scFv-FP approach can be particularly useful for labeling proteins that are sensitive to C'-terminal FP fusion, such as Rfa1.⁴¹ We have demonstrated that while Rfa1-Envy fusion leads to increased yeast sensitivity to a DNA-damaging agent and cytoplasmic Rfa1 aggregation, the labeling of Rfa1-3HA or Rfa1-6HA with 2E2-NLS-Envy does not compromise yeast viability and Rfa1 function (Figures 3 and S3). Furthermore, the enhanced detection of RPA foci in the labeled Rfa1-HA strains highlights the advantage of this approach for functional C'-terminal protein labeling relative to direct Rfa1-GFP fusion. A key feature of this labeling approach for the enhanced detection of DNA damage is the low expression level of the scFv-FP fusion. Low scFv-FP expression that is independent of the target protein expression leads to reduced nuclear background fluorescence. Indeed, the increased detection of 2E2-Envy-labeled RPA or Rad52 foci, following DNA-damage induction (Figures 2 and 3), is correlated with low nuclear fluorescence background (Figures S2 and S3).

The application of the scFv-FP approach for labeling HA-tagged proteins located at different cellular organelles including nuclear membrane, peroxisome, the Golgi apparatus, and the mitochondria demonstrates the potential of the scFv-FP to serve as a general tool for the fluorescent labeling of HA-tagged yeast proteins. This can be particularly important since it is estimated that more than two thirds of the yeast proteome is localized in the cytoplasm, cytoplasmic organelles, or membranes.⁶⁷

In addition, yeast has been extensively used as a model organism for the study of eukaryotic membrane organelles due to the high conservation of key proteins located in these organelles.⁵² The dual usage of HA-tagged proteins for fluorescent microscopy and immunological assays including WB analysis reduces the experimental effort devoted for strain construction.

In summary, we have developed an easily adaptable approach for fluorescent labeling of proteins in live yeast cells. We have constructed and utilized a series of integrative plasmids expressing scFvs-FPs (Figure S1A) for the flexible labeling of tagged yeast proteins localized to different organelles in the yeast cell. We believe that future scFv-FP labeling of a variety of additional HA-tagged yeast proteins can significantly promote yeast research that rely on live-cell fluorescent microscopy for the examination of the function and localization of cellular proteins.

Limitations of the study

In the case of proteins that are sensitive to C-terminal FP fusion (e.g., Rfa1) or proteins generating large complexes (e.g., Rad52), substoichiometric labeling of HA-tagged proteins results in signal intensities that are similar to direct fusion of the protein to Envy. Thus, in these cases, amplification of the protein fluorescent signal is not achieved. In addition, since many yeast strains expressing HA-tagged proteins are widely used for WB and chromatin immunoprecipitation (ChIP) analysis, these HA-tagged strains can be easily transformed using the integrative plasmids described here (Figure S1A) for the live-cell imaging examination of a wide variety of cellular proteins. However, a potential limitation of using plasmids for HA tagging can stem from the possible negative effect of the 3xHA tag on protein stability.⁶⁸ Finally, this method does not enable labeling of proteins with diffuse cytoplasmic localization or proteins targeted to organelles with limited access for the scFv-FP.

STAR★METHODS

Detailed methods are provided in the online version of this paper and include the following:

- KEY RESOURCES TABLE
- RESOURCE AVAILABILITY
 - Lead contact
 - Materials availability
 - Data and code availability
- EXPERIMENTAL MODEL AND SUBJECT DETAILS
 - *Saccharomyces cerevisiae* strain generation
- METHOD DETAILS
 - Plasmids construction
 - Microscopy
 - DNA damage induction
 - Yeast growth assays
 - Western blot
- QUANTIFICATION AND STATISTICAL ANALYSIS

SUPPLEMENTAL INFORMATION

Supplemental information can be found online at <https://doi.org/10.1016/j.crmeth.2022.100357>.

ACKNOWLEDGMENTS

We thank Justin Greenblat for his help in designing the HA-tag codon sequences and Maya Schuldiner for providing the N terminus GFP-labeled Rfa1 strain. We thank Dikla Nachmias and Natalie Elia for their assistance with the confocal microscopy experiments. I.T. thanks his wife, his family, and his cat for their support. This work was supported by the Israel Science Foundation (ISF) grant numbers 1340/17, 2359/18, and 707/21 and the Binational Science Foundation (BSF-NSF) grant number 2019617.

AUTHOR CONTRIBUTIONS

Conceptualization, I.T., D.D., and A.A.; methodology, I.T., T.Z., A.C., and L.R.; investigation, I.T., T.Z., and A.A.; writing, I.T. and A.A.; funding acquisition, A.A.; resources, A.C. and D.D.; supervision, A.A.

DECLARATION OF INTERESTS

The authors declare no competing interests.

INCLUSION AND DIVERSITY

One or more of the authors of this paper self-identifies as a member of the LGBTQIA+ community.

Received: April 26, 2022

Revised: September 19, 2022

Accepted: November 10, 2022

Published: December 6, 2022

REFERENCES

- Burgess, S.M., Powers, T., and Mell, J.C. (2017). Budding Yeast *Saccharomyces Cerevisiae* as a Model Genetic Organism. *eLS*, 1–12. <https://doi.org/10.1002/9780470015902.a0000821.pub2>.
- Karathia, H., Vilaprinyo, E., Sorribas, A., and Alves, R. (2011). *Saccharomyces cerevisiae* as a model organism: a comparative study. *PLoS One* 6, e16015. <https://doi.org/10.1371/journal.pone.0016015>.
- Schekman, R. (2010). Charting the secretory pathway in a simple eukaryote. *Mol. Biol. Cell* 21, 3781–3784. <https://doi.org/10.1091/mbc.E10-05-0416>.
- Day, R.N., and Davidson, M.W. (2009). The fluorescent protein palette: tools for cellular imaging. *Chem. Soc. Rev.* 38, 2887–2921. <https://doi.org/10.1039/b901966a>.
- Day, R.N., and Schaufele, F. (2008). Fluorescent protein tools for studying protein dynamics in living cells: a review. *J. Biomed. Opt.* 13, 031202. <https://doi.org/10.1117/1.2939093>.
- Huh, W.-K., Falvo, J.V., Gerke, L.C., Carroll, A.S., Howson, R.W., Weissman, J.S., and O'Shea, E.K. (2003). Global analysis of protein localization in budding yeast. *Nature* 425, 686–691. <https://doi.org/10.1038/nature02026>.
- Slubowski, C.J., Funk, A.D., Roesner, J.M., Paulissen, S.M., and Huang, L.S. (2015). Plasmids for C-terminal tagging in *Saccharomyces cerevisiae* that contain improved GFP proteins, *Envy* and *Ivy*. *Yeast* 32, 379–387. <https://doi.org/10.1002/yea.3065>.
- Lee, S., Lim, W.A., and Thorn, K.S. (2013). Improved blue, green, and red fluorescent protein tagging vectors for *S. cerevisiae*. *PLoS One* 8, e67902–e67911. <https://doi.org/10.1371/journal.pone.0067902>.
- Zhao, X., Li, G., and Liang, S. (2013). Several affinity tags commonly used in chromatographic purification. *J. Anal. Methods Chem.* 2013, 581093. <https://doi.org/10.1155/2013/581093>.
- Costantini, L.M., Baloban, M., Markwardt, M.L., Rizzo, M.A., Guo, F., Verkhusha, V.V., and Snapp, E.L. (2015). A palette of fluorescent proteins optimized for diverse cellular environments. *Nat. Commun.* 6, 7670. <https://doi.org/10.1038/ncomms8670>.
- Wiedenmann, J., Oswald, F., and Nienhaus, G.U. (2009). Fluorescent proteins for live cell imaging: opportunities, limitations, and challenges. *IUBMB Life* 61, 1029–1042. <https://doi.org/10.1002/iub.256>.
- Freidel, C., Kaloyanova, S., and Peneva, K. (2016). Chemical tags for site-specific fluorescent labeling of biomolecules. *Amino Acids* 48, 1357–1372. <https://doi.org/10.1007/s00726-016-2204-5>.
- Li, C., Tebo, A.G., and Gautier, A. (2017). Fluorogenic labeling strategies for biological imaging. *Int. J. Mol. Sci.* 18, E1473. <https://doi.org/10.3390/ijms18071473>.
- Liu, J., and Cui, Z. (2020). Fluorescent labeling of proteins of interest in live cells: beyond fluorescent proteins. *Bioconjug. Chem.* 31, 1587–1595. <https://doi.org/10.1021/acs.bioconjchem.0c00181>.
- Weill, U., Krieger, G., Avihou, Z., Milo, R., Schuldiner, M., and Davidi, D. (2019). Assessment of GFP tag position on protein localization and growth fitness in yeast. *J. Mol. Biol.* 431, 636–641. <https://doi.org/10.1016/j.jmb.2018.12.004>.
- Demchenko, A.P. (2020). Photobleaching of organic fluorophores: quantitative characterization, mechanisms, protection. *Methods Appl. Fluoresc.* 8, 022001. <https://doi.org/10.1088/2050-6120/ab7365>.
- Weill, U., Yofe, I., Sass, E., Stynen, B., Davidi, D., Natarajan, J., Ben-Menachem, R., Avihou, Z., Goldman, O., Harpaz, N., et al. (2018). Genome-wide SWAp-Tag yeast libraries for proteome exploration. *Nat. Methods* 15, 617–622. <https://doi.org/10.1038/s41592-018-0044-9>.
- Ramm, K., Gehrig, P., and Plückerthun, A. (1999). Removal of the conserved disulfide bridges from the scFv fragment of an antibody: effects on folding kinetics and aggregation. *J. Mol. Biol.* 290, 535–546. <https://doi.org/10.1006/jmbi.1999.2854>.
- Boersma, S., Khuperkar, D., Verhagen, B.M.P., Sonneveld, S., Grimm, J.B., Lavis, L.D., and Tanenbaum, M.E. (2019). Multi-color single-molecule imaging uncovers extensive heterogeneity in mRNA decoding. *Cell* 178, 458–472.e19, e19. <https://doi.org/10.1016/j.cell.2019.05.001>.
- Liu, Y., Zhao, N., Kanemaki, M.T., Yamamoto, Y., Sadamura, Y., Ito, Y., Tokunaga, M., Stasevich, T.J., and Kimura, H. (2021). Visualizing looping of two endogenous genomic loci using synthetic zinc-finger proteins with anti-FLAG and anti-HA frankenbodies in living cells. *Gene Cell.* 26, 905–926. <https://doi.org/10.1111/gtc.12893>.
- Tanenbaum, M.E., Gilbert, L.A., Qi, L.S., Weissman, J.S., and Vale, R.D. (2014). A protein-tagging system for signal amplification in gene expression and fluorescence imaging. *Cell* 159, 635–646. <https://doi.org/10.1016/j.cell.2014.09.039>.
- Zhao, N., Kamijo, K., Fox, P.D., Oda, H., Morisaki, T., Sato, Y., Kimura, H., and Stasevich, T.J. (2019). A genetically encoded probe for imaging nascent and mature HA-tagged proteins *in vivo*. *Nat. Commun.* 10, 2947. <https://doi.org/10.1038/s41467-019-10846-1>.
- Murakawa, T., Nakamura, T., Kawaguchi, K., Murayama, F., Zhao, N., Stasevich, T.J., Kimura, H., and Fujita, N. (2022). A *Drosophila* toolkit for HA-tagged proteins unveils a block in autophagy flux in the last instar larval fat body. *Development* 149, dev200243. <https://doi.org/10.1242/dev.200243>.
- Viswanathan, S., Williams, M.E., Bloss, E.B., Stasevich, T.J., Speer, C.M., Nern, A., Pfeiffer, B.D., Hooks, B.M., Li, W.P., English, B.P., et al. (2015). High-performance probes for light and electron microscopy. *Nat. Methods* 12, 568–576. <https://doi.org/10.1038/nmeth.3365>.
- Peng, B., Williams, T.C., Henry, M., Nielsen, L.K., and Vickers, C.E. (2015). Controlling heterologous gene expression in yeast cell factories on different carbon substrates and across the diauxic shift: a comparison of yeast promoter activities. *Microb. Cell Fact.* 14, 1–11. <https://doi.org/10.1186/s12934-015-0278-5>.
- Adam, S.A., Lobl, T.J., Mitchell, M.A., and Gerace, L. (1989). Identification of specific binding proteins for a nuclear location sequence. *Nature* 337, 276–279. <https://doi.org/10.1038/337276a0>.

27. Dovrat, D., Dahan, D., Sherman, S., Tsirkas, I., Elia, N., and Aharoni, A. (2018). A live-cell imaging approach for measuring DNA replication rates. *Cell Rep.* *24*, 252–258. <https://doi.org/10.1016/j.celrep.2018.06.018>.
28. Robinett, C.C., Straight, A., Li, G., Wilhelm, C., Sudlow, G., Murray, A., and Belmont, A.S. (1996). *In vivo* localization of DNA sequences and visualization of large-scale chromatin organization using lac operator/repressor recognition. *J. Cell Biol.* *135*, 1685–1700. <https://doi.org/10.1083/jcb.135.6.1685>.
29. Straight, A.F., Belmont, A.S., Robinett, C.C., and Murray, A.W. (1996). GFP tagging of budding yeast chromosomes reveals that protein-protein interactions can mediate sister chromatid cohesion. *Curr. Biol.* *6*, 1599–1608. [https://doi.org/10.1016/s0960-9822\(02\)70783-5](https://doi.org/10.1016/s0960-9822(02)70783-5).
30. Dahan, D., Tsirkas, I., Dovrat, D., Sparks, M.A., Singh, S.P., Galletto, R., and Aharoni, A. (2018). Pif1 is essential for efficient replisome progression through lagging strand G-quadruplex DNA secondary structures. *Nucleic Acids Res.* *46*, 11847–11857. <https://doi.org/10.1093/nar/gky1065>.
31. Tsirkas, I., Dovrat, D., Lei, Y., Kalyva, A., Lotysh, D., Li, Q., and Aharoni, A. (2021). Cac1 WHD and PIP domains have distinct roles in replisome progression and genomic stability. *Curr. Genet.* *67*, 129–139. <https://doi.org/10.1007/s00294-020-01113-8>.
32. Tsirkas, I., Dovrat, D., Thangaraj, M., Brouwer, I., Cohen, A., Paleiov, Z., Meijler, M.M., Lenstra, T., and Aharoni, A. (2022). Transcription-replication coordination revealed in single live cells. *Nucleic Acids Res.* *50*, 2143–2156. <https://doi.org/10.1093/nar/gkac069>.
33. Lisby, M., and Rothstein, R. (2004). DNA damage checkpoint and repair centers. *Curr. Opin. Cell Biol.* *16*, 328–334. <https://doi.org/10.1016/j.ceb.2004.03.011>.
34. Lisby, M., and Rothstein, R. (2005). Localization of checkpoint and repair proteins in eukaryotes. *Biochimie* *87*, 579–589. <https://doi.org/10.1016/j.biochi.2004.10.023>.
35. Brill, S.J., and Stillman, B. (1991). Replication factor-A from *Saccharomyces cerevisiae* is encoded by three essential genes coordinately expressed at S phase. *Genes Dev.* *5*, 1589–1600. <https://doi.org/10.1101/gad.5.9.1589>.
36. Longhese, M.P., Neecke, H., Paciotti, V., Lucchini, G., and Plevani, P. (1996). The 70 kDa subunit of replication protein A is required for the G1/S and intra-S DNA damage checkpoints in budding yeast. *Nucleic Acids Res.* *24*, 3533–3537. <https://doi.org/10.1093/nar/24.18.3533>.
37. Bélanger, F., Angers, J.P., Fortier, É., Hammond-Martel, I., Costantino, S., Drobetsky, E., and Wurtele, H. (2016). Mutations in replicative stress response pathways are associated with S phase-specific defects in nucleotide excision repair. *J. Biol. Chem.* *291*, 522–537. <https://doi.org/10.1074/jbc.M115.685883>.
38. Srikumar, T., Lewicki, M.C., Costanzo, M., Tkach, J.M., van Bakel, H., Tsui, K., Johnson, E.S., Brown, G.W., Andrews, B.J., Boone, C., et al. (2013). Global analysis of SUMO chain function reveals multiple roles in chromatin regulation. *J. Cell Biol.* *201*, 145–163. <https://doi.org/10.1083/jcb.201210019>.
39. Breker, M., Gymrek, M., Moldavski, O., and Schuldiner, M. (2014). LoQAtE - localization and Quantitation ATlas of the yeast proteome. A new tool for multiparametric dissection of single-protein behavior in response to biological perturbations in yeast. *Nucleic Acids Res.* *42*, 726–730. <https://doi.org/10.1093/nar/gkt933>.
40. Dhingra, N., Wei, L., and Zhao, X. (2019). Replication protein A (RPA) sumoylation positively influences the DNA damage checkpoint response in yeast. *J. Biol. Chem.* *294*, 2690–2699. <https://doi.org/10.1074/jbc.RA118.006006>.
41. Yates, L.A., Aramayo, R.J., Pokhrel, N., Caldwell, C.C., Kaplan, J.A., Perera, R.L., Spies, M., Antony, E., and Zhang, X. (2018). A structural and dynamic model for the assembly of Replication Protein A on single-stranded DNA. *Nat. Commun.* *9*, 5447. <https://doi.org/10.1038/s41467-018-07883-7>.
42. Beranek, D.T. (1990). Distribution of methyl and ethyl adducts following alkylation with monofunctional alkylating agents. *Mutat. Res.* *231*, 11–30. [https://doi.org/10.1016/0027-5107\(90\)90173-2](https://doi.org/10.1016/0027-5107(90)90173-2).
43. Henke, R.M., Dastidar, R.G., Shah, A., Cadinu, D., Yao, X., Hooda, J., and Zhang, L. (2011). Hypoxia elicits broad and systematic changes in protein subcellular localization. *Am. J. Physiol. Cell Physiol.* *301*, C913–C928. <https://doi.org/10.1152/ajpcell.00481.2010>.
44. Bai, Y., and Symington, L.S. (1996). A Rad52 homolog is required for RAD51-independent mitotic recombination in *Saccharomyces cerevisiae*. *Genes Dev.* *10*, 2025–2037. <https://doi.org/10.1101/gad.10.16.2025>.
45. Game, J.C. (1993). DNA double-strand breaks and the RAD50-RAD57 genes in *Saccharomyces*. *Semin. Cancer Biol.* *4*, 73–83.
46. Lisby, M., Rothstein, R., and Mortensen, U.H. (2001). Rad52 forms DNA repair and recombination centers during S phase. *Proc. Natl. Acad. Sci. USA.* *98*, 8276–8282. <https://doi.org/10.1073/pnas.121006298>.
47. Kagawa, W., Kurumizaka, H., Ishitani, R., Fukai, S., Nureki, O., Shibata, T., and Yokoyama, S. (2002). Crystal structure of the homologous-pairing domain from the human Rad52 recombinase in the undecameric form. *Mol. Cell* *10*, 359–371. [https://doi.org/10.1016/S1097-2765\(02\)00587-7](https://doi.org/10.1016/S1097-2765(02)00587-7).
48. Rout, M.P., Aitchison, J.D., Suprpto, A., Hjertaas, K., Zhao, Y., and Chait, B.T. (2000). The yeast nuclear pore complex: composition, architecture, transport mechanism. *J. Cell Biol.* *148*, 635–651. <https://doi.org/10.1083/jcb.148.4.635>.
49. Strambio-De-Castillia, C., Niepel, M., and Rout, M.P. (2010). The nuclear pore complex: bridging nuclear transport and gene regulation. *Nat. Rev. Mol. Cell Biol.* *11*, 490–501. <https://doi.org/10.1038/nrm2928>.
50. Nazarko, T.Y. (2017). Pexophagy is responsible for 65% of cases of peroxisome biogenesis disorders. *Autophagy* *13*, 991–994. <https://doi.org/10.1080/15548627.2017.1291480>.
51. Ma, C., Agrawal, G., and Subramani, S. (2011). Peroxisome assembly: matrix and membrane protein biogenesis. *J. Cell Biol.* *193*, 7–16. <https://doi.org/10.1083/jcb.201010022>.
52. Zhu, J., Zhang, Z.-T., Tang, S.-W., Zhao, B.-S., Li, H., Song, J.-Z., Li, D., and Xie, Z. (2019). A validated set of fluorescent-protein-based markers for major organelles in yeast (*Saccharomyces cerevisiae*). *mBio* *10*, 016911–19.
53. Thakur, J.K., Arthanari, H., Yang, F., Chau, K.H., Wagner, G., and Näär, A.M. (2009). Mediator subunit Gal11p/MED15 is required for fatty acid-dependent gene activation by yeast transcription factor Oaf1p. *J. Biol. Chem.* *284*, 4422–4428. <https://doi.org/10.1074/jbc.M808263200>.
54. Truscott, K.N., Brandner, K., and Pfanner, N. (2003). Mechanisms of protein import into mitochondria. *Curr. Biol.* *13*, 326–337. [https://doi.org/10.1016/S0960-9822\(03\)00239-2](https://doi.org/10.1016/S0960-9822(03)00239-2).
55. Mokranjac, D., and Neupert, W. (2009). Thirty years of protein translocation into mitochondria: unexpectedly complex and still puzzling. *Biochim. Biophys. Acta* *1793*, 33–41. <https://doi.org/10.1016/j.bbamcr.2008.06.021>.
56. Liu, Q., Cheng, L., Matsuura, A., Xiang, L., and Qi, J. (2020). Gentiopicroside, a secoiridoid glycoside from *Gentiana rigescens* franch, extends the lifespan of yeast via inducing mitophagy and antioxidative stress. *Oxid. Med. Cell. Longev.* *2020*, 9125752. <https://doi.org/10.1155/2020/9125752>.
57. Nishioka, K., Ohtsubo, T., Oda, H., Fujiwara, T., Kang, D., Sugimachi, K., and Nakabeppu, Y. (1999). Expression and differential intracellular localization of two major forms of human 8-oxoguanine DNA glycosylase encoded by alternatively spliced OGG1 mRNAs. *Mol. Biol. Cell* *10*, 1637–1652. <https://doi.org/10.1091/mbc.10.5.1637>.
58. Campbell, C.L., and Thorsness, P.E. (1998). Escape of mitochondrial DNA to the nucleus in yme1 yeast is mediated by vacuolar-dependent turnover of abnormal mitochondrial compartments. *J. Cell Sci.* *111*, 2455–2464. <https://doi.org/10.1242/jcs.111.16.2455>.
59. Frazier, A.E., Taylor, R.D., Mick, D.U., Warscheid, B., Stoepel, N., Meyer, H.E., Ryan, M.T., Guiard, B., and Rehling, P. (2006). Mdm38 interacts with

- ribosomes and is a component of the mitochondrial protein export machinery. *J. Cell Biol.* 172, 553–564. <https://doi.org/10.1083/jcb.200505060>.
60. Lyon, K., and Stasevich, T.J. (2017). Imaging translational and post-translational gene regulatory dynamics in living cells with antibody-based probes. *Trends Genet.* 33, 322–335. <https://doi.org/10.1016/j.tig.2017.02.003>.
61. Wang, C., Han, B., Zhou, R., and Zhuang, X. (2016). Real-time imaging of translation on single mRNA transcripts in live cells. *Cell* 165, 990–1001. <https://doi.org/10.1016/j.cell.2016.04.040>.
62. Wu, B., Eliscovich, C., Yoon, Y.J., and Singer, R.H. (2016). Translation dynamics of single mRNAs in live cells and neurons. *Science* 352, 1430–1435. <https://doi.org/10.1126/science.aaf1084>.
63. Morisaki, T., Lyon, K., DeLuca, K.F., DeLuca, J.G., English, B.P., Zhang, Z., Lavis, L.D., Grimm, J.B., Viswanathan, S., Looger, L.L., et al. (2016). Real-time quantification of single RNA translation dynamics in living cells. *Science* 352, 1425–1429. <https://doi.org/10.1126/science.aaf0899>.
64. Yan, X., Hoek, T.A., Vale, R.D., and Tanenbaum, M.E. (2016). Dynamics of translation of single mRNA molecules *in vivo*. *Cell* 165, 976–989. <https://doi.org/10.1016/j.cell.2016.04.034>.
65. Stasevich, T.J., Hayashi-Takanaka, Y., Sato, Y., Maehara, K., Ohkawa, Y., Sakata-Sogawa, K., Tokunaga, M., Nagase, T., Nozaki, N., McNally, J.G., and Kimura, H. (2014). Regulation of RNA polymerase II activation by histone acetylation in single living cells. *Nature* 516, 272–275. <https://doi.org/10.1038/nature13714>.
66. Lenstra, T.L., Coulon, A., Chow, C.C., and Larson, D.R. (2015). Single-molecule imaging reveals a switch between spurious and functional ncRNA transcription. *Mol. Cell* 60, 597–610. <https://doi.org/10.1016/j.molcel.2015.09.028>.
67. Kumar, A., Agarwal, S., Heyman, J.A., Matson, S., Heidtman, M., Piccirillo, S., Umansky, L., Drawid, A., Jansen, R., Liu, Y., et al. (2002). Subcellular localization of the yeast proteome. *Genes Dev.* 16, 707–719. <https://doi.org/10.1101/gad.970902>.
68. Saiz-Baggetto, S., Méndez, E., Quilis, I., Igual, J.C., and Bañó, M.C. (2017). Chimeric proteins tagged with specific 3xHA cassettes may present instability and functional problems. *PLoS One* 12, e0183067. <https://doi.org/10.1371/journal.pone.0183067>.
69. Soreanu, I., Hendler, A., Dahan, D., Dovrat, D., and Aharoni, A. (2018). Marker-free genetic manipulations in yeast using CRISPR/CAS9 system. *Curr. Genet.* 64, 1129–1139. <https://doi.org/10.1007/s00294-018-0831-y>.
70. Gibson, D.G., Young, L., Chuang, R.-Y., Venter, J.C., Hutchison, C.A., and Smith, H.O. (2009). Enzymatic assembly of DNA molecules up to several hundred kilobases. *Nat. Methods* 6, 343–345. <https://doi.org/10.1038/nmeth.1318>.

STAR★METHODS

KEY RESOURCES TABLE

REAGENT or RESOURCE	SOURCE	IDENTIFIER
Antibodies		
Mouse anti-HA-tag mAb (F-7)	Santa Cruz	Cat# sc-7392; RRID:AB_627809
Mouse anti-PGK1 mAb	Invitrogen	Cat# 459250; RRID:AB_2532235
Goat anti-Mouse IgG (H + L) Secondary Antibody, HRP	Thermo Fisher Scientific	Cat# 32430; RRID:AB_1185566
Chemicals, peptides, and recombinant proteins		
Difco™ Yeast Nitrogen Base w/o AAs (YNB) (powder)	Becton, Dickinson and Company	Cat# 291940
Bacto™ Agar (powder)	Becton, Dickinson and Company	Cat# 214010
Bacto™ Yeast extract (powder)	Becton, Dickinson and Company	Cat# 212750
Bacto™ Peptone (powder)	Becton, Dickinson and Company	Cat# 211677
YPD Broth (powder)	Formedium	Cat# CCM0210
D-(+)-Glucose, Anhydrous, 99% (powder)	Alfa Aesar	Cat# A16828
Drop-out Mix Complete (powder)	US Biological Life Sciences	Cat# D9515
G418 Disulphate Salt (G418) (powder)	Formedium	Cat# G4185
Hygromycin B (HYG) (powder)	Formedium	Cat# HYG5000
5-Fluoro Orotic Acid Monohydrate (5-FOA) (powder)	Formedium	Cat# 5FOA05
Nourseothricin Sulfate (ClonNAT) (powder)	GoldBio	Cat# N-500-3
Water (H ₂ O)	Sigma-Aldrich	Cat# 7732-18-5
Agarose (powder)	Life Gene	Cat# LAG0701
SYBR Safe DNA Gel Stain	Invitrogen	Cat# S33102
TAE Buffer 50x	Biolab	Cat# 002050232300
Sodium Hydroxide 98% (NaOH) (powder)	Acros Organics	Cat# 134070010
Herring Sperm DNA (liquid)	Promega	Cat# D1816
Lithium Acetate Dihydrate (LiAc) (powder)	Sigma-Aldrich	Cat# L6883
Poly(Ethylene Glycol) 3,350 (PEG) (powder)	Sigma-Aldrich	Cat# P4338
Acrylamide/Bis-Acrylamide 29:1 40%	Biolab	Cat# 1382333500
Tris hydrochloride (powder)	Thermo Fisher Scientific	Cat# BP153-1
SDS Solution 10%	Biological Industries	Cat# 01-890-1B
Glycerol Anhydrous	Biolab	Cat# 000712050100
TEMED	BioRad	Cat# 1610801
Ammonium Persulfate (APS)	Acros Organics	Cat# 327081000
Bromophenol Blue	BioRad	Cat# 161-0404
2-Mercaptoethanol 99% pure	Acros Organics	Cat# 125472500
TGS Buffer 10x	BioLab	Cat# 20522323
Dulbecco's Phosphate Buffered Saline (PBS)	Biological Industries	Cat# 02-023-5A
Tween20	Sigma-Aldrich	Cat# P1379-500ML
Albumin	BioBasic	Cat# 9048-46-8
Trans-Blot Turbo PVDF membranes Midi 0.2 μm PVDF Transfer Packs	BioRad	Cat# 1704157
Skim milk powder	Sigma-Aldrich	Cat# 70166-500G

(Continued on next page)

REAGENT or RESOURCE	SOURCE	IDENTIFIER
EZ-ECL Chemiluminescence detection kit	Biological Industries	Cat# 20-500-120
Methyl methane-sulfonate (MMS)	Sigma-Aldrich	Cat# 129925-5G
Ethanol (EtOH)	JT Baker	Cat# 64-17-5
Dimethyl Sulfoxide (DMSO)	Thermo Fisher Scientific	Cat# BP231-100
Oleic Acid	Sigma-Aldrich	Cat# O1383-1G
Tween80	Sigma-Aldrich	Cat# P1754-500
Mitotracker Red CMXRos	Invitrogen	Cat# M7512
Hoechst 33342 Trihydrochloride, Trihydrate	Thermo Fisher Scientific	Cat# H3570
Concanavalin A (ConA) (powder)	Sigma-Aldrich	Cat# L7647
α -Mating factor Acetate Salt (powder)	Sigma-Aldrich	Cat# T6901
SiR-HALO	Tsirkas et al. ³²	N/A
Critical commercial assays		
KOD Hot Start DNA Polymerase	Millipore	Cat# 71086-3
KAPA Polymerase and Buffers	Roche	Cat# 07958846001
ALLIn™ RED Taq Mastermix 2x	HighQu	Cat# PCM0201c1
DreaMTaq Green PCR Master Mix 2x	Thermo Fisher Scientific	Cat# K1081
Nucleospin® Plasmid Easy Pure	Macherey-Nagel	Cat# 740727
Nucleospin® Gel and PCR Clean-up	Macherey-Nagel	Cat# 740609
NEBuilder® HiFi DNA Assembly Master Mix	New England Biolabs	Cat# E2621X
Deposited data		
Microscopy images	This manuscript	https://doi.org/10.5281/zenodo.7215514
Original Western Blot images	This manuscript	https://doi.org/10.5281/zenodo.7214898
Experimental models: Organisms/strains		
<i>Saccharomyces cerevisiae</i> W1588	Dhingra et al. ⁴⁰	N/A
Oligonucleotides		
DNA oligos for PCR amplification and plasmid construction	IDT and Sigma-Aldrich	N/A
Recombinant DNA		
Plasmids for scFv-FP integration and expression	This manuscript	N/A
Plasmids for -3HAtag or -6HAtag protein labeling	This manuscript	N/A
Software and algorithms		
Matlab (version R2019b)	Mathworks	https://www.mathworks.com/products.html?s_tid=gn_ps
Python (versions 2.7 and 3.8)	Python	https://www.python.org
PyCharm (2020.2)	JetBrains	https://www.jetbrains.com/pycharm/
ZEN (version 3.0 blue edition)	Zeiss	https://www.micro-shop.zeiss.com/en/us/softwarefinder/#select-soft-ware
ImageJ	ImageJ	https://imagej.net/downloads
DotQuant	Dovrat et al. ²⁷	https://doi.org/10.5281/zenodo.7304362
TokyoGhoulRe (foci/background identification and quantification)	This manuscript	https://doi.org/10.5281/zenodo.7214818
EldenRing (nuclear membrane identification and quantification)	This manuscript	https://doi.org/10.5281/zenodo.7214832
Other		
μ -Slide 8 Well Uncoated	Ibidi	Cat# 80821
petri dishes	Greiner Bio-one	Cat# 633 102
PCR strip tubes	Axygen	Cat# PCR-0208-C

(Continued on next page)

Continued

REAGENT or RESOURCE	SOURCE	IDENTIFIER
PCR tubes	Axygen	Cat# PCR-02-A
Cuvettes	Alex Red	Cat# CUV010015
Weighing paper	Bar Naor Ltd	Cat# BN70081L
Laboratory Film	Parafilm	Cat# PM-996
Eclipse™ Pipet Tips 10-20μL	Labcon	Cat# 1036-260-000-9
Eclipse™ Pipet Tips 100-200-250μL	Labcon	Cat# 1093-260-000-9
Eclipse™ Pipet Tips 1000-1250μL	Labcon	Cat# 1045-260-000-9SSS
Discovery Comfort Pipette 0.5–10 μL, 2–20 μL, 20–200 μL, 100–1000μL	HTL	Cat# 7901
5 mL pipettes	Costar	Cat# 4487
10 mL pipettes	Sorfa	Cat# 314100
25 mL pipettes	Sorfa	Cat# 315100
1.5 mL plastic tubes	FL Medical	Cat# 23053
1.5 mL black plastic tubes	N/A	Cat# HS4323K
50 mL plastic tubes	N/A	Cat# 227270
Quadloops PS	N/A	Cat# 8150032001
Filters 0.22 μm (200-5000-1000mL)	N/A	N/A
Cell Spreaders	N/A	N/A
Plastic Volumetric Cylinders (100 -500-1000mL)	N/A	N/A
Glass Bottles (250 -500-1000mL)	N/A	N/A
Microscope Stand Axio Observer 7	Zeiss	Cat# 431007-9904-000
Scanning Stage 130x100 STEP (D)	Zeiss	Cat# 432029-9904-000
Stage Controller XY STEP SMC 2009	Zeiss	Cat# 432929-9011-000
Solid-State Light Source Colibri 7	Zeiss	Cat# 423052-9741-000
Photometrics sCMOS Prime BSI imaging camera	Zeiss	Cat# 01-PRIME-BSI-R-M-16-C
Trans Blot Turbo transfer system	Bio Rad	Cat# 1704150
Fusion Fx Vilber Lourmat	A ₂ S	N/A
Nanodrop 2000 Spectrophotometer	Thermo Fisher Scientific	N/A
Tabletop Microcentrifuge MicroCL 17R	Thermo Fisher Scientific	N/A
Tabletop Centrifuge5810R for 50 mL tubes	Lumitron	N/A
Weighing Scale	Presica	N/A
Analytical Scale	Sartorius	N/A
C1000 Touch Thermal Cycler	BioRad	N/A
Vortex Genie 2	Scientific Industries	N/A
SevenEasy™ pH Meter	Mettel Toledo	N/A
Biophotometer	Eppendorf	N/A
Microwave oven	N/A	N/A

RESOURCE AVAILABILITY

Lead contact

Further information and requests for resources and reagents should be directed to and will be fulfilled by the lead Contact, Amir Aharoni (aaharoni@bgu.ac.il).

Materials availability

Plasmids for scFv-FP integration and expression and plasmids for -3HAtag or -6HAtag protein labeling generated in this study are available upon request. SiR-HALO dye sample is available upon request.

Data and code availability

- Microscopy images and original western blot images have been deposited at Zenodo and are publicly available as of the date of publication. DOIs are listed in the [key resources table](#). Microscopy and any additional data reported in this paper will be shared by the [lead contact](#) upon request.
- All original code has been deposited at Zenodo and is publicly available as of the date of publication. DotQuant code is available upon request. DOIs are listed in the [key resources table](#).
- Any additional information required to reanalyze the data reported in this paper is available from the [lead contact](#) upon request.

EXPERIMENTAL MODEL AND SUBJECT DETAILS

Saccharomyces cerevisiae strain generation

All yeast strains were generated on the background of W1588 MATa strain, which is identical to W303 but with a wild-type copy of Rad5.⁴⁰ In strains for FROS imaging, *lacOx128* and *tetOx128* non-repetitive arrays were integrated at *chrIV*:332960 and *chrIV*:352560 respectively, adjacent to *ARS413*. Additionally, *PDR5* was deleted in these strains using *hphMX* cassette. A sequence for the expression of LacI-HALO in the nucleus was integrated to the *pdr5* locus using a markerless CRISPR-Cas9 approach targeting the *hphMX* antibiotic cassette.⁶⁹ *PEX6* and *MDM38* genes were replaced by *natMX* cassette. Fusion of Envy or mKate2 to the C' termini of target proteins was performed by integrating a PCR cassette containing the fluorescent protein and an antibiotic marker for selection at the 3' of the gene. Yeast transformations were performed with standard LiAc transformation protocol. Replacements and integrations were validated by PCR followed by standard sequencing.

METHOD DETAILS

Plasmids construction

To construct the scFv-FP containing plasmids, we cloned 15F11, 2E2 and gp41Nb^{19,22} into a plasmid containing Envy⁷ or YO version of mKate2⁸ under control of 1) a weak, 175 bp segment of the *URA3* promoter, 2) the 623 bp *RPL15A* promoter, or 3) the strong 700 bp *ADH1* promoter.²⁵ The scFvs were fused to the FPs with a GS-rich linker and either with or without an NLS sequence. *CYC1* or *ADH1* terminators were used for the efficient termination of scFv-Envy and scFv-mKate2 transcription. The *kanMX* or *hphMX* antibiotic cassettes were inserted downstream or upstream of the scFv-FP constructs. Finally, these plasmids contain homology regions with the *ADE1* locus for their efficient genomic integration following restriction with *SrfI*.

To construct plasmids containing the epitope repeats for the C' tagging of proteins in yeast, a GS-rich linker followed by three or six repeats of HA-tag and the *TRP1* terminator were integrated in pAG25 and pAG32, upstream of *natMX* or *hphMX* cassettes, respectively. Alternatively, the linker, the HA-tags or Moon-tags followed by *TRP1* terminator were integrated in a *kanMX* containing plasmid, for selection with *G418*. The tags HA- or Moon- are separated by eight GS-rich linkers that are encoded by variable DNA sequences, such that each linker has a different sequence. This minimizes the repetitive nature of the tags to ensure the multi-tag sequence will be stable and easy to amplify by PCR. All plasmids were generated with Gibson Assembly reaction (NEB).⁷⁰ The full collection of the plasmids for scFv-FP expression and plasmids for HA or Moon-tag are available upon request.

Microscopy

Yeast cells were grown overnight in synthetic complete (SC) medium containing 4% glucose (GLC) at 30°C. Yeast cultures were then diluted to O.D.₆₀₀ = 0.2 and were grown for 2 hr before imaging in microscopy slide chambers (Ibidi). For replication-time experiments, yeast cultures were diluted at O.D.₆₀₀ = 0.1 and SiR-HALO dye was added to a final concentration of 800 nM.³² Synchronization at G1 phase was initiated 1 hour following SiR-HALO dye addition, by adding 10 µg/mL α -factor (Genscript) and the cultures were incubated for two additional hours. For nucleus staining, cell cultures were incubated with 10 µg/mL Hoechst 33432 (Thermo Fisher Scientific) for 30 min. For mitochondria labeling, Tom70-labeled cells were incubated with 100 nM Mitotracker Red CMXRos dye (Invitrogen) for 30-45 min. Cells were immobilized on microscopy slide chambers (Ibidi) coated with 2 mg/mL concanavalin A (Sigma-Aldrich) and washed thoroughly from α -factor and SiR-HALO dye, or Hoechst and Mitotracker dyes with warm SC medium containing 4% GLC prior to microscopy experiments. Live-cell imaging of the cells was performed on an AxioObserver inverted wide-field microscope (Zeiss) with a Colibri 7 LED light source at 30°C using a x63 oil objective (NA = 1.4) in 3D (8 or 12 z-sections, 0.8 µm apart). Hoechst, Envy, mKate2 or Mitotracker, and SiR-HALO were excited with 385 nm, 488 nm, 600 nm, and 650 nm illumination, respectively. For time-lapse experiments, cells were imaged at 1 min intervals for 3 hours. mKate2-labeled nucleoporins were imaged using a ZEISS confocal microscope.

DNA damage induction

For the induction of DNA damage, yeast cells were grown overnight in SC 4% GLC media at 30°C. Yeast cells were diluted at O.D.₆₀₀ = 0.15 and were grown for 3 additional hours. Next, cells were immobilized on microscopy slide chambers coated with 2 mg/mL concanavalin A. For the induction of DNA damage, cells were irradiated under the microscope with high-intensity 385 nm illumination every 90 sec for 30 min. The number of nuclear Rfa1 or Rad52 foci was counted before and after irradiation,

as well as the total number of total cells on the microscopy slide to calculate the percentage of foci identified in each experiment. All experiments were performed in triplicates.

Yeast growth assays

For yeast growth experiments, overnight cultures in YPD (Formedium) were diluted to $O.D._{600} = 0.08$ in triplicates and the $O.D._{600}$ was measured every hour until yeast reached an $O.D._{600}$ of ≈ 1.2 – 2.0 . For drop assay experiments, overnight yeast cultures were diluted to $O.D._{600} = 0.15$ in YPD and were grown for three additional hours. Cells were diluted to $O.D._{600} = 0.3$ and 4 μ L were transferred in YPD agar plates in the presence or absence of 0.005–0.01% MMS, in YPO plates (1% yeast extract, 2% peptone, 0.2% oleic acid, 0.02% Tween 80, and 2% agar) or in YPEG plates (1% yeast extract, 2% peptone, 3% glycerol, 3% ethanol, and 2% agar) in 10-fold serial dilutions. Plates were photographed after 24 hr (YPD), 48 hr (YPD + MMS and YPEG), or 72 hr (YPO). All growth experiments were performed at 30°C.

Western blot

Proteins tagged with HA were detected with Western Blot (WB) as previously described.³² Briefly, 50 mL of yeast cells were grown until late-exponential phase ($O.D._{600} \approx 1$). Cells were centrifuged and pellets were frozen at -80°C overnight. Next day, cell pellets were resuspended and incubated in 1 mL of 0.2 M NaOH (Acros Organics) for 5 min in room temperature (RT), followed by boiling at 95°C for 5 min in 100 μ L of Laemmli Buffer including 10% β -mercaptoethanol (Acros Organics). Lysates were centrifuged for 2 min and 4 μ L of the supernatants were loaded and run on 10% SDS-PAGE gel for approximately 2 h at 120–150 V. Separated protein bands were transferred to PVDF membranes (BioRad) followed by blocking with PBST +10% skim milk (Sigma Aldrich) overnight at 4°C on a roller mixer. Membranes were washed with PBST once for 2 min and incubated for 1 h with a primary mouse anti-HA antibody (1:1000) (Santa Cruz Biotechnologies) or a primary mouse anti-Pgk1 antibody (1:5000) (Invitrogen) in PBST +10% skim milk. Then, membranes were washed three times with PBST for 5 min each and were incubated for 1 h with a secondary goat-anti-mouse antibody (1:10000) conjugated with HRP (Thermo Fisher Scientific). Bands of the HA tagged proteins or Pgk1 were detected with the EZ-ECL Chemiluminescence detection kit (Biological Industries) according to manufacturer's protocol.

QUANTIFICATION AND STATISTICAL ANALYSIS

Quantification of *tetO* and *lacO* dot intensities and estimation of replication times in single cells was done as previously described.²⁷ Briefly, real-time fluorescent measurements were collected with ZEN 3.0 and analyzed using a custom-made MATLAB pipeline developed for the analysis of replication rates. This analysis allows the identification, tracking, and quantification of the LacI-Halo-SiR and tetR-Envy or 2E2-NLS-Envy labeled tetR-3HA dots in each cell. Statistical analysis of replication time data and foci intensity were performed using Monte Carlo resampling with 1,000,000 iterations.²⁷

Rfa1 or Rad52 foci intensities, peroxisome foci, and Golgi apparatus puncta intensities were calculated using a combined custom-made MATLAB-ImageJ script. The nuclear fluorescent intensity in Rfa1 and Rad52 strains was calculated with a modified version of this MATLAB-ImageJ script, using the foci as reference. For Rad52-Envy or Rad52-3HA/6HA labeled with 2E2-Envy and Rad52-yomKate2 foci colocalization, we analyzed cells containing both Envy and mKate2 foci and we scored them for the colocalization of the two foci species. Then, for each replicate, we divided the number of cells where the foci were colocalized with the total number of cells which we examined. Nuclear membrane intensity of labeled Nup-HA cells were estimated using a custom-made MATLAB script. Tom70 intensity was measured using masking in ImageJ. Foci and nuclear membrane intensity in different strains were compared using Monte Carlo resampling with 1,000,000 iterations. Cell percentage with Rfa1 and Rad52 foci were compared using student's T-test. Swarm plots, violin plots, and growth curves were plotted using the Seaborn package in Python. Bar graphs were plotted with Microsoft Office Excel 2016.